

©1996 IEEE. Personal use of this material is permitted. However, permission to reprint/republish this material for advertising or promotional purposes or for creating new collective works for resale or redistribution to servers or lists, or to reuse any copyrighted component of this work in other works must be obtained from the IEEE.

Copyright and all rights therein are retained by authors or by other copyright holders. All persons copying this information are expected to adhere to the terms and constraints invoked by each author's copyright. In most cases, these works may not be reposted without the explicit permission of the copyright holder.

This copyright notice is taken from the IEEE PSPB Operations Manual, section 8.1.10 entitled "Electronic Information Dissemination". At the time of this notice, this section is posted at

http://www.ieee.org/portal/index.jsp?pageID=corp_level1&path=about/documentation/copyright&file=policies.xml&xsl=generic.xsl

Noise Analysis of a Continuous-Time Auto-Zeroed Amplifier

Ivars G. Finvers, James W. Haslett, *Senior Member, IEEE*, and F. N. Trofimenkoff, *Senior Member, IEEE*

Abstract—The effect of auto-zeroing on the internal noise of a continuous-time auto-zeroed amplifier is analyzed and a set of empirical expressions are developed which predict the important aspects of its noise shaping behavior. The dependence of the output noise power spectral density on the auxiliary signal path gain, nulling amplifier bandwidth, and auto-zeroing clock frequency are all demonstrated. The results are confirmed experimentally.

I. INTRODUCTION

AUTO-ZEROED AMPLIFIERS are used primarily in instrumentation applications that require the precise measurements of slowly varying signals. In such applications the accuracy with which measurements can be made depends on both the input offset voltage and the low frequency noise power spectral density (PSD). The auto-zeroing technique is an attractive means of building a precision amplifier since it allows the construction of an amplifier with low input offset voltage in a standard CMOS fabrication process without the need for precision components or trimming [1]–[3]. An auto-zeroed amplifier suitable for continuous-time applications is shown in Fig. 1.

The same sampling and subtraction process used by an auto-zeroed amplifier to reduce its input offset voltage also modifies the shape of the amplifier's output noise PSD. Our research has shown that, as demonstrated in Fig. 2, the shape of the low frequency noise PSD of an auto-zeroed amplifier depends strongly upon the bandwidth of the nulling amplifier. When the nulling amplifier bandwidth is similar to or greater than the auto-zeroing clock frequency, the output noise PSD plateaus at low frequency and the level of the plateau increases with decreasing clock frequency. On the other hand, if the nulling amplifier bandwidth is much less than the clock frequency, the PSD shows a humped shape at low frequencies which is largely independent of clock rate. In both cases the low frequency noise PSD level is less than the level that would be present if no auto-zeroing had been applied to the main amplifier. This paper describes a set of empirically derived expressions

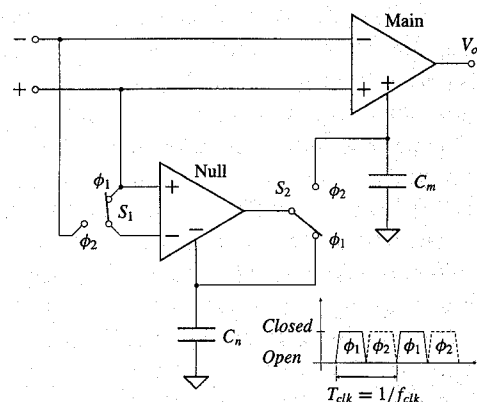


Fig. 1. Continuous-time auto-zeroed amplifier.

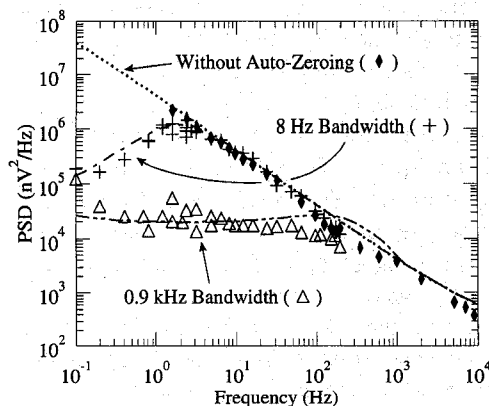


Fig. 2. Measured noise PSD of an auto-zeroed amplifier which shows variation of low frequency noise with nulling amplifier bandwidth. The auto-zeroing clock frequency is 1000 Hz. Markers indicate measured data.

which model the noise shaping characteristics of a continuous-time auto-zeroed amplifier. These expressions allow the circuit designer to obtain insight into how the amplifier's parameters influence its noise PSD.

Two classes of auto-zeroed amplifiers exist: discrete-time and continuous-time. Discrete-time auto-zeroed amplifiers process the signal on one clock phase and zero their offset during the other clock phase. Since the amplifier must be removed from the signal path periodically, discrete-time amplifiers are best suited to applications such as switched capacitor circuits. The continuous-time auto-zeroed amplifier, which is shown in Fig. 1, is more complex as it requires two amplifiers. During one clock phase the nulling amplifier zeroes its own offset voltage and then on the next clock phase it zeros the main amplifier offset voltage. The main

Manuscript received March 14, 1995; revised November 1, 1995. This work was supported by the Alberta Microelectronic Centre, the Natural Sciences and Engineering Research Council of Canada, the Alberta Heritage Scholarship Fund, and the Izaak Walter Killiam Memorial Fund. This paper was recommended by Associate Editor D. A. Johns.

I. G. Finvers was with the Department of Electrical and Computer Engineering, University of Calgary, Calgary, Alberta, Canada T2N 1N4. He is now with Mitel Semiconductor, Ottawa, Ontario, Canada K2K 1X3.

J. W. Haslett and F. N. Trofimenkoff are with the Department of Electrical and Computer Engineering, University of Calgary, Calgary, Alberta, Canada T2N 1N4.

Publisher Item Identifier S 1057-7130(96)07637-9.

amplifier always remains in the signal path and processes the input signal continuously. The effective offset voltage of the overall amplifier, after auto-zeroing, can be shown to be approximately

$$V_{os,eff} \simeq \frac{V_{os,m}(\alpha_m/\alpha_n)}{A'_{on}} + \frac{V_{os,n}}{A'_{on}} \quad (1)$$

where $V_{os,m}$ and $V_{os,n}$ are the inherent offset voltages of the main and nulling amplifiers, respectively, α_m and α_n are the ratio of the primary and auxiliary path open loop gains of main and nulling amplifiers, respectively, (these are discussed in more detail in Section II), and A'_{on} is the open loop gain from the auxiliary input of the nulling amplifier to its output. Second-order effects have been neglected in (1); a more detailed analysis can be found in [4] and [5].

Since offset voltage is no different than very low frequency noise, it is expected that the low frequency noise of the auto-zeroed amplifier should also be reduced. The auto-zeroing process bears a strong similarity to the correlated double sampling (CDS) process originally developed to reduce reset noise in CCD's [6]. The noise performance of CDS circuits has been treated extensively in the literature [6]–[9] while the noise analysis of the discrete-time auto-zeroed amplifier has been carried out by Enz [10]. Discrete-time auto-zeroed amplifiers are used primarily in switched capacitor circuits and therefore the rate of auto-zeroing is very fast—at the same clock rate as the switched capacitor network—requiring that the amplifier have a wide bandwidth. The rate of auto-zeroing in a continuous-time auto-zeroed amplifier is much lower and consequently the bandwidth of the nulling amplifier is typically very low. The difference in the nulling amplifier bandwidth between a discrete and continuous-time auto-zeroed amplifier has a significant effect on the noise analysis. A complete noise analysis of the continuous-time auto-zeroed amplifier which includes such effects as the variation of the low frequency noise PSD shape with nulling amplifier bandwidth as demonstrated in Fig. 2 is not available in the published literature. This paper provides such an analysis.

In analyzing the noise performance of the auto-zeroed amplifier, the time-varying nature of the circuit must be considered. At first glance it may seem that the circuit could be analyzed in a straightforward fashion with Z -transforms using the same methods as are used for switched-capacitor circuits. This is not the case since the bandwidth of the nulling amplifier is potentially below the sampling frequency. Low bandwidth implies that the hold capacitors may not fully charge or discharge within one switching interval. As noted by Liou [11] for the case of switched capacitor circuits with nonideal operational amplifiers, the circuit behavior must be modeled using differential equations. The periodically switched nature of the circuit simplifies the analysis allowing general closed form solutions of the network's frequency response to be obtained. These were obtained first by Liou [12] for a sinusoidal input (of the form $Ae^{j\omega t}$) and then by Strom and Signell [13] for an arbitrary input.

Although closed form solutions for the frequency response of a periodically switched network can be obtained using the methods of Strom and Signell, the results are in general very

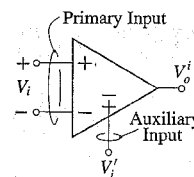


Fig. 3. Four port amplifier.

complicated in analytical form and are tractable for only the simplest circuits. Therefore, to analyze the noise performance of the continuous-time auto-zeroed amplifier we first applied the analytical techniques developed by Strom and Signell to a simplified model of the amplifier. The resulting equations were then solved numerically to obtain a simulation of the noise performance of the amplifier.

Noise simulations however only provide a means of checking the performance of an amplifier *after* it has been designed. What is more useful to a designer during the initial design process are analytical expressions which relate amplifier parameters to noise behavior. In Section III we present a set of empirical expressions which describe the important characteristics of the noise transfer functions. A brief discussion of the development and origin of these expressions is provided. Before the noise transfer functions can be discussed it is necessary to provide models for both the auto-zeroed amplifier and the noise sources. This is done in Section II. The correctness of the noise simulations and empirical expressions is verified against experimental data in Section IV, which also includes a discussion of the results and their implications for amplifier design.

II. MODELS

For this analysis the simplified model of the auto-zeroed amplifier shown in Fig. 1 is used. The switches are controlled by a two-phase nonoverlapping clock. The main and nulling amplifiers are four port amplifiers with both a primary input and an auxiliary input as defined in Fig. 3. The auxiliary input is used to apply the offset correction signal to each amplifier. To minimize the offset voltage, the nulling and main amplifiers are usually designed to be identical [5] except that the main amplifier has an additional output stage to provide load drive capability. This assumption simplifies the analysis somewhat.

The output voltage of each of the amplifiers (Fig. 3) can be expressed as

$$V_o^i(s) = (V_i + V_i'/\alpha + V_{os})A(s) \quad (2)$$

where V_i and V_i' are the input voltages that are applied to the primary and auxiliary inputs, respectively, and V_{os} is the offset voltage of the amplifier referred to its primary input. Throughout this paper primed symbols are used to denote parameters belonging to the auxiliary input, whereas the subscript modifiers m and n denote parameters belonging to the main and nulling amplifiers, respectively. Both the main and nulling amplifiers are designed to be dominant pole, so that the gain from the primary input of each amplifier to its output

can be modeled as

$$A(s) = \frac{V_o^i}{V_i} = \frac{A_o}{1 + s/\omega_d} \quad (3)$$

where A_o is the dc open loop gain and ω_d is the dominant pole. The high frequency poles of the amplifier are not important in this investigation and are therefore neglected. The auxiliary input usually has the same poles as the primary input but will have a different open loop dc gain A'_o . This assumption is valid for most implementations in which the auxiliary and primary input signals are combined within the first stage of the amplifier, a common practice. Defining the ratio of the open loop dc gains between the primary and auxiliary inputs as $\alpha = A_o/A'_o$, the open loop gain from the auxiliary input of each amplifier to its output will be

$$A'(s) = \frac{V_o^i}{V_i'} = \frac{A(s)}{\alpha} \quad (4)$$

A. Noise Model

To keep the analysis tractable only a system level noise analysis of the auto-zeroed amplifier is performed. The main and nulling amplifiers are each represented by a simplified small signal equivalent circuit along with an equivalent input referred noise source. The device level calculation of the equivalent input noise source for each amplifier has been treated extensively elsewhere [15], [16] and will not be considered here.

Each amplifier is modeled as a 4-port network. In general, a noisy linear N -port network can be replaced by a noiseless N -port network along with a noise source at each port [17]. The noise sources can be either a voltage source in series with each port, a current source shunting each port, or some combination of voltage and current sources.

Since auto-zeroed amplifiers are typically constructed in CMOS technology, we choose a noise model based on voltage sources, as shown in Fig. 4(a). It is generally accepted [18], [15], [16] that MOSFET low frequency noise can be represented by an equivalent input referred noise voltage source connected in series with the gate terminal. A factor which further simplifies the development of the noise model is the very high input impedance of the MOSFET gate terminal. Each of the amplifier input terminals is connected to the gate of a MOSFET. The high input impedance of the gate ensures that the noise contributions of the amplifier's internal transistors are independent of the impedance of the input signal sources. (At high frequencies the isolation of the internal transistors from the influence of the source impedance will weaken due to coupling through the gate capacitance, but our interest lies primarily in low frequency noise performance where the assumption of isolation is reasonable.)

Assuming that the contribution at low frequencies of the four noise sources in Fig. 4(a) to the output noise is independent of input source impedance, a simpler noise model consisting of only a single input referred noise source can be used, as shown in Fig. 4(b). The single noise source model is also commonly used for the standard 3-port MOS amplifier [15], [16].

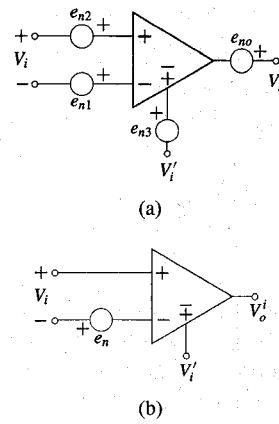


Fig. 4. (a) General noise model for a four port amplifier. (b) Simplified model.

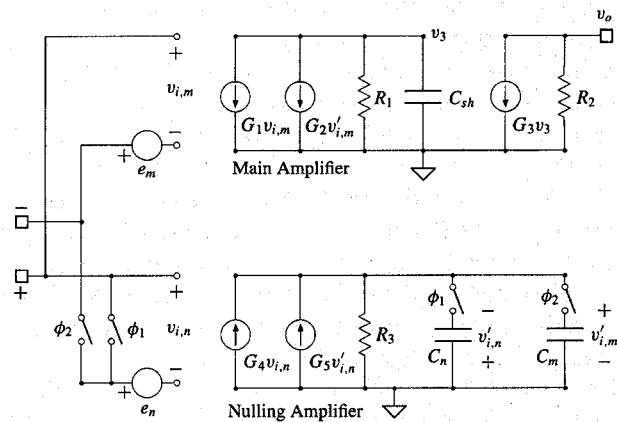


Fig. 5. Small signal model used for noise analysis.

B. Small Signal Model

To keep the analysis tractable, the simplified small signal model shown in Fig. 5 is used for the auto-zeroed amplifier.

From the small signal model, the important amplifier parameters that will be used in later discussions can be derived. The open loop gains of the primary and auxiliary inputs for both the main and nulling amplifier are

$$A_{sh} = \frac{v_{o,m}}{v_{i,m}} = G_1 R_1 G_3 R_2 \quad (5)$$

$$A'_{om} = \frac{v_{o,m}}{v'_{i,m}} = G_2 R_1 G_3 R_2 \quad (6)$$

$$A_{on} = \frac{v_{o,n}}{v_{i,n}} = G_4 R_3 \quad (7)$$

$$A'_{on} = \frac{v_{o,n}}{v'_{i,n}} = G_5 R_3 \quad (8)$$

the gain ratios are given by

$$\alpha_m = \frac{A_{om}}{A'_{om}} = \frac{G_1}{G_2}, \quad \alpha_n = \frac{A_{on}}{A'_{on}} = \frac{G_4}{G_5} \quad (9)$$

and the dominant poles are

$$\omega_{dm} = \frac{1}{R_1 C_{sh}}, \quad \omega_{dn} = \frac{1}{R_3 C_m} \quad (10)$$

III. NOISE ANALYSIS

It can be shown that the frequency domain response of a linear periodically switched network to an arbitrary input signal is of the form [13]

$$Y(f) = \sum_{x=-\infty}^{\infty} |T_x(f)|^2 S(f - x f_{\text{clk}}) \quad (11)$$

where S and Y are the Fourier transforms of the input and output signals, and f_{clk} is the switching frequency. Equation (11) shows that the output frequency response of a periodically switched network contains weighted and frequency translated images of the input signal. T_0 represents the transfer function of the network for the baseband input signal, while $T_{x, x \neq 0}$ are the transfer functions for the frequency translated images that result from the switching action. The determination of the output response potentially requires the summation of an infinite number of image components. However, in most practical cases bandwidth limitations within the circuit limit the number of nonnegligible T_x 's to a finite and summable number.

Although Strom and Signell [13] showed that it is possible to obtain a closed form solution for the transfer functions T_x , in practice symbolic solutions are unmanageable for all but the simplest circuits. Therefore we analyzed the noise shaping characteristics of the continuous-time auto-zeroed amplifier by applying Strom and Signell's methods to the state equations which describe the amplifier in each of its two switching states and then solving the resultant equations numerically. This approach has the advantage over using a general purpose simulator such as SPICE in that the amplifier noise PSD's are calculated directly. Numerical solutions are however of limited usefulness since they are valid only for a specific set of amplifier parameters. To obtain a more general result we have devised a set of empirical equations from the numerical results which describe the key aspects of the amplifier noise transfer characteristics. These equations help the designer to understand how changes in amplifier parameters will impact noise performance.

Since the details of the numerical solutions are not of great importance to this discussion they are omitted. The interested reader is referred to [5] for the complete details.

In this analysis the contributions to the total noise appearing at the output of the main amplifier due to the input referred noise voltage sources of both the main (e_m) and nulling (e_n) amplifiers are calculated. Since the auto-zeroed amplifier must operate in a closed loop configuration, the noise analysis is performed with the amplifier configured with a feedback factor of $1/\beta$.

The equations which follow have been derived empirically. In general, only the most important characteristics have been modeled and only the envelope of the magnitude characteristic has been considered. *No phase information* can be obtained from the following models.

In all of the following models it is assumed that the amplifier is operating with frequency independent feedback (β is a constant) and the switching clock has a 50% duty cycle.

A. Transfer Functions for $x = 0$

An important contribution to the total output noise comes from the baseband component, that is, the term $|T_0|^2 S(f)$ in (11). It was found from analysing the simulation results that the transfer functions for the baseband signal components ($x = 0$) can be approximated by

$$T_0^{e_n}(f) \approx \frac{1}{\beta} \frac{1}{A'_{\text{on}}} \frac{(1 + jf/f_a)}{(1 + jf/f_b)} \frac{1}{(1 + jf/f_c)} \quad (12)$$

$$T_0^{e_m}(f) \approx \frac{1}{\beta} \frac{1}{A'_{\text{on}} \alpha_n / \alpha_m} \frac{(1 + jf/f_d)}{(1 + jf/f_e)} \frac{1}{(1 + jf/\beta f_f)} \quad (13)$$

where $T_x^{e_n}$ and $T_x^{e_m}$ are the transfer functions from the input referred noise sources of the nulling and main amplifiers respectively to the output. Referring to the small signal model given in Fig. 5, the poles and zeros are given by

$$f_a = \frac{f_b}{G_5 R_3} = \frac{f_b}{A'_{\text{on}}} \quad (14)$$

$$f_b = \frac{1}{4\pi C_n / G_5 + \pi / (4\sqrt{2} f_{\text{clk}})} \quad (15)$$

$$f_c = \frac{G_5}{4\pi C_m} \quad (16)$$

$$f_d = \frac{f_e}{G_2 G_4 R_3 / G_1} = \frac{f_b}{A'_{\text{on}} \alpha_n / \alpha_m} \quad (17)$$

$$f_e = \frac{1}{4\pi G_1 C_m / (G_2 G_4) + \pi / (4\sqrt{2} f_{\text{clk}})} \quad (18)$$

$$f_f = \frac{G_1 G_3 R_2}{2\pi C_{sh}} \quad (19)$$

Fig. 6 shows that the shape of the T_0 's predicted by the empirical equations closely resembles those obtained by simulation for a variety of different amplifier models (defined in Tables I and II). The defining characteristic of amplifier model #1 is the low bandwidth of the nulling amplifier, in this aspect it is representative of most continuous-time auto-zeroed amplifiers. Amplifier model #2 is identical to #1 except that the nulling amplifier bandwidth is significantly higher. The third and fourth amplifier models are used to illustrate the effect on noise of using a high clock frequency and having a high nulling amplifier bandwidth (during ϕ_1).

Consider the nulling amplifier noise source transfer characteristic that is given in (12). At low frequencies the noise transferred to the output behaves in a manner analogous to the input offset voltage (see (1)). This can be understood intuitively by realizing that the noise which is present in the frequency band much lower than the auto-zeroing clock frequency will be highly correlated between samples. The noise sampled during ϕ_1 is strongly correlated to the noise from which the sample is subtracted during ϕ_2 . Therefore, the low frequency noise level is reduced by the same factor of A'_{on} as the offset voltage.

Equation (12) also indicates that the overall noise level is increased by the noise gain $1/\beta$ of the external feedback circuit as expected. The pole f_c models the high frequency noise attenuation due to the nulling amplifier closed loop bandwidth. The pole f_c occurs at one half the nominal bandwidth of the nulling amplifier during ϕ_2 since the noise is passed to the

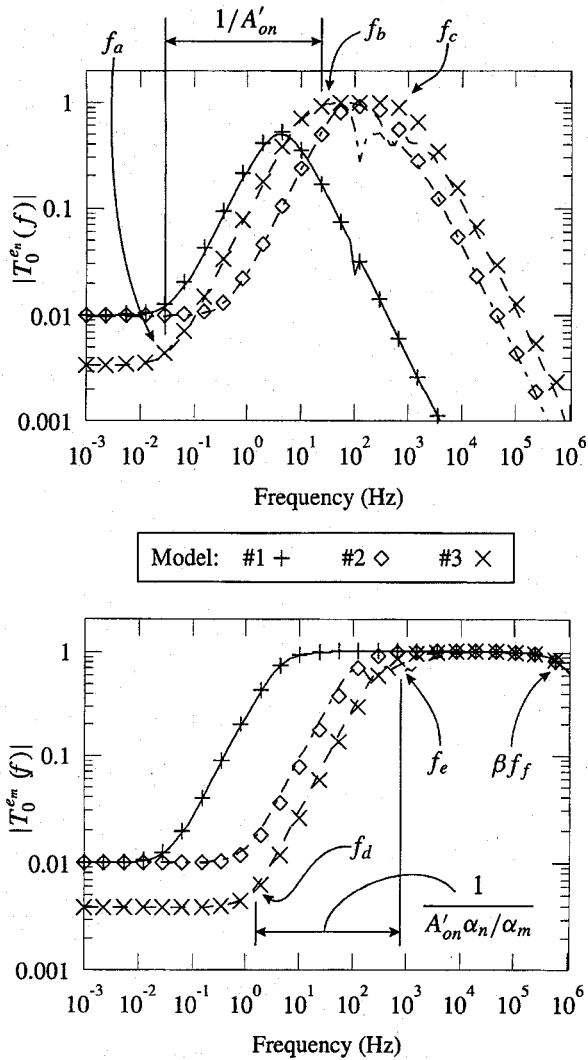


Fig. 6. Comparison of the baseband transfer functions generated by simulation (lines) with those derived from the empirical models (markers) for the noise sources e_n (top) and e_m (bottom). The amplifier models used for the comparison are given in Table II. Also indicated are the approximate locations of the transfer function poles and zeros for the transfer functions calculated using model #3.

main output only 50% of the time. This reduction in bandwidth due to switching is similar to that shown by Kaehler [21] for a switched RC low-pass filter where the filter's time constant was reduced to $\tau_{\text{switched}} = \chi RC$ when switched with a duty cycle of χ .

The pole f_b represents the upper frequency limit for which the auto-zeroing process will reduce the noise. This pole consists of two components. The component $G_5/4\pi C_n$ is the closed loop bandwidth of the nulling amplifier during ϕ_1 (again decreased by a factor of 2 due to the 50% duty cycle) and is dominant only if it is significantly below the auto-zeroing clock frequency. In this situation the nulling amplifier behaves like a low-pass filter with a bandwidth of $G_5/4\pi C_n$. Model #1 illustrates this in Fig. 6 (note that for model #1 the pole $f_c < f_b$). However, if the nulling amplifier bandwidth is greater than the clock frequency, the auto-zeroing process will only be effective in reducing noise for frequencies up to approximately $4\sqrt{2}f_{\text{clk}}/\pi$. This is the same frequency

limit that is obtained for the ideal discrete-time auto-zeroed amplifier analyzed in Appendix A (which the nulling amplifier begins to approximate once its bandwidth exceeds the clock frequency) [10], [5]. In Fig. 6 the curves belonging to amplifier model #3 illustrate the secondary limit being reached by pole f_b .

The zero f_a is the transition point at which the noise reduction due to auto-zeroing begins to decrease from the maximum level of $1/A'_{\text{on}}$ due to the reduction in the nulling amplifier auxiliary path loop gain.

The origins of the poles and zeros of the main amplifier baseband transfer function $T_0^{e_m}$ are very similar to those of $T_0^{e_n}$. The primary difference being that βf_f , the closed loop bandwidth of the main amplifier, is typically much greater than f_c since it depends on the main amplifier compensation capacitor instead of the much larger hold capacitor. The maximum noise reduction at low frequencies is determined by the same $A'_{\text{on}}\alpha_n/\alpha_m$ factor as the level of offset voltage reduction.

Equations (12) and (13) predict the approximate shape of the baseband transfer functions but omit the fine details. For example the "nulls" in $T_0^{e_n}$ which occur at the odd multiples of f_{clk} are not modeled. Also, for very small $C_{m|n}$, $T_0^{e_n}$ overestimates the magnitude of the response by a factor of 2 for frequencies greater than f_{clk} . However, the equations are accurate enough for their intended purpose, i.e., design.

B. Transfer Functions for $x \neq 0$

The transfer functions of the frequency translated noise components are split into two groups, even and odd, based on the index x . The odd transfer functions are typically much stronger than the even ones, especially when the nulling amplifier bandwidth is low (usually this corresponds to the use of large $C_{m|n}$'s). Empirically, for $x \neq 0$ and odd x , it was found that for a 50% duty cycle the transfer functions can be approximated by

$$T_x^{e_n} \approx \frac{1}{\beta} \left[\frac{j}{x\pi} + \frac{\coth(G_5/4C_n f_{\text{clk}})}{(1 - j2\pi x C_n f_{\text{clk}}/G_5)} + \frac{\coth(G_5/4C_m f_{\text{clk}})}{2(1 - j2\pi n C_m f_{\text{clk}}/G_5)} \right] \frac{1}{(1 + j4\pi f C_m/G_5)} \quad (20)$$

$$T_x^{e_m} \approx \frac{1}{\beta} \left[\frac{j}{x\pi} + \frac{1}{2(1 - j2\pi x C_m f_{\text{clk}}/G_5)} \right] \times \frac{1}{(1 + j4\pi f C_m/G_5)} \quad (21)$$

while for $x \neq 0$ and even x

$$T_x^{e_n} \approx \frac{1}{\beta} \left[\frac{1}{(1 - j2\pi x C_n f_{\text{clk}}/G_5)} - \frac{1}{2(1 - j2\pi x C_m f_{\text{clk}}/G_5)} \right] \frac{1}{(1 + j2\pi f C_m/G_5)} \quad (22)$$

$$T_x^{e_m} \approx \frac{1}{\beta} \left[\frac{1}{2(1 - j2\pi x C_m f_{\text{clk}}/G_5)} \right] \frac{1}{(1 + j2\pi f C_m/G_5)} \quad (23)$$

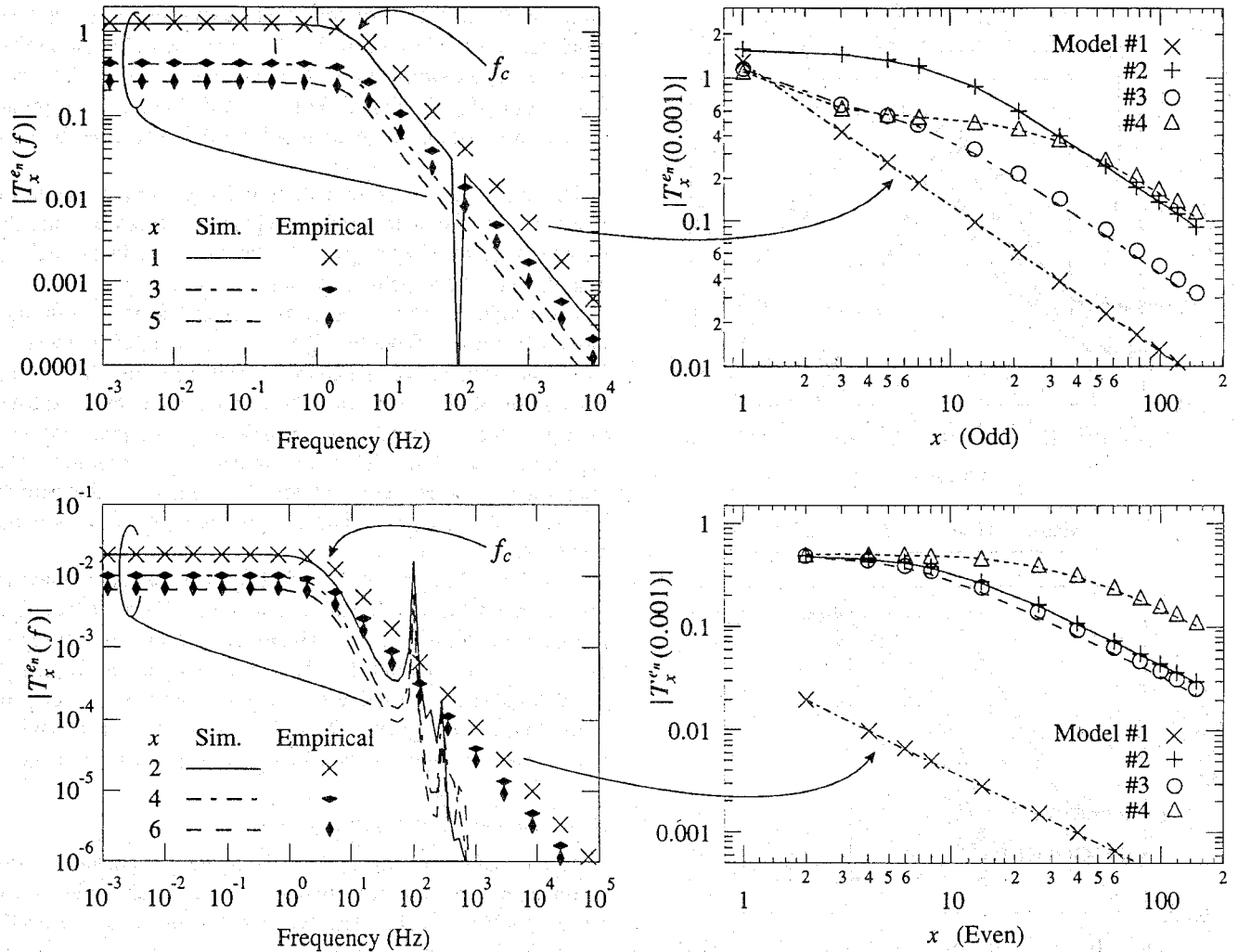


Fig. 7. Frequency dependence of $T_{x,x \neq 0}^{en}$ is demonstrated for model #1 of Table I. The transfer functions for the first three odd and even x are shown in the top left and bottom left graphs respectively. Simulated results are indicated with lines while the markers show the values predicted by (20) and (22). The two right-hand graphs show the very low frequency dependence (calculated at $f = 0.001$ Hz) of $T_{x,x \neq 0}^{en}$ for a selection of the model parameters given in Table I.

A comparison of the empirical and simulation results for these transfer functions is shown in Fig. 7 for a variety of amplifier models. The frequency dependent roll-off in (20)–(23) is modeled in a straightforward fashion as the closed loop bandwidth of the nulling amplifier (with an extra factor of 2 appearing in (20) and (21) due to the 50% duty cycle). This model underestimates the frequency roll-off, especially when x is even, but is adequate for the design process. A more accurate model of the roll-off could not be found. Aspects of the transfer functions not modeled by the empirical expressions are the nulls and peaks which occur at multiples of the clock frequency. Simulations show that these components do not represent an important contribution to the overall noise PSD and can therefore be neglected.

The dependence on x of the $T_{x,x \neq 0}$'s is complicated and the initial guess of its form was obtained from the equivalent transfer function of the simplified discrete-time auto-zeroed amplifier that is given by (34) in Appendix A. To highlight the dependence of (34) on x , the frequency dependent portion of the expression can be eliminated by taking its limit as $f \rightarrow 0$.

For odd x the limit of (34) is

$$\frac{j}{x\pi} + \frac{\coth(1/4RCf_{\text{clk}})}{2(1 - j2\pi xRCf_{\text{clk}})} \quad (24)$$

while for even x it is

$$\frac{-1}{2(1 - j2\pi xRCf_{\text{clk}})} \quad (25)$$

To apply these results to the continuous-time auto-zeroed amplifier the R in (24) and (25), which corresponds to the output resistance of the discrete-time auto-zeroed amplifier, is replaced with $1/G_5$, the output resistance of the nulling amplifier under closed loop conditions. After this substitution, the resulting expressions form the base from which the equations given in (20)–(23) were devised.

IV. EXPERIMENTAL VERIFICATION AND INTERPRETATION

The low frequency noise power spectral density of the test amplifier (which is described in detail in [5]) was measured and compared with the the PSD computed using the switched network analysis described in Section III. The measured and

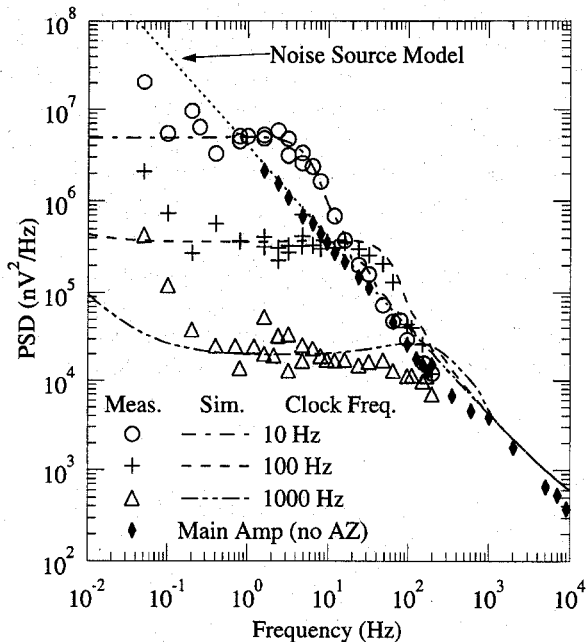


Fig. 8. Measured and simulated output noise PSD for the test amplifier with a nulling amplifier bandwidth of 250 Hz, corresponding to hold capacitor of $C_{m|n} = 980$ pF. Measured data points are indicated by markers while lines are used for the calculated PSD.

simulated noise PSD's are compared in Figs. 8 and 9 for three clock frequencies (10, 100, and 1000 Hz) and two hold capacitor sizes (0.98 and 100 nF). The simulation results include the noise contributions of the aliased terms over the range of $-20 \leq x \leq 20$. The amplifier parameters used in the computation of the PSD's are given by model #5 in Table I. These parameters are derived from the measured performance of the test amplifier, and correspond to an amplifier with $A_{on} \approx 10^4$, $A'_{om} \approx 4 \times 10^3$, $\alpha_{m|n} \approx 100$, and a GBW $\approx 5 \times 10^6$. The noise model used for the input referred noise PSD of both the main and nulling amplifiers is

$$S_e = 200 \left(1 + \frac{2 \times 10^4}{|f|} \right) \text{ nV}^2/\text{Hz}. \quad (26)$$

This noise model assumes that the dominant source of the noise is the input stage. Otherwise, the noise at high frequencies would need to increase to properly model the contributions of the noise sources in the output stage that are not attenuated by to the amplifier's limited bandwidth. Potentially such high frequency noise could be aliased down into baseband by the circuit switching action and increase the overall noise level. However such behavior was not observed experimentally and was therefore neglected. The coefficients of the noise source model were determined by curve fitting the expression $S_{no}(1 + f_k/|f|)$ to the measured noise PSD of the main amplifier. To measure the main amplifier PSD, the clock was stopped in ϕ_2 and the auxiliary input terminal was connected to ac ground. In this configuration, the noise at the output is that due to the inherent noise of the main amplifier alone. Assuming that the main amplifier inherent noise is dominated by the noise of the input stage, it is a reasonable to assume that the nulling amplifier noise can also be approximated by the same noise model as the main

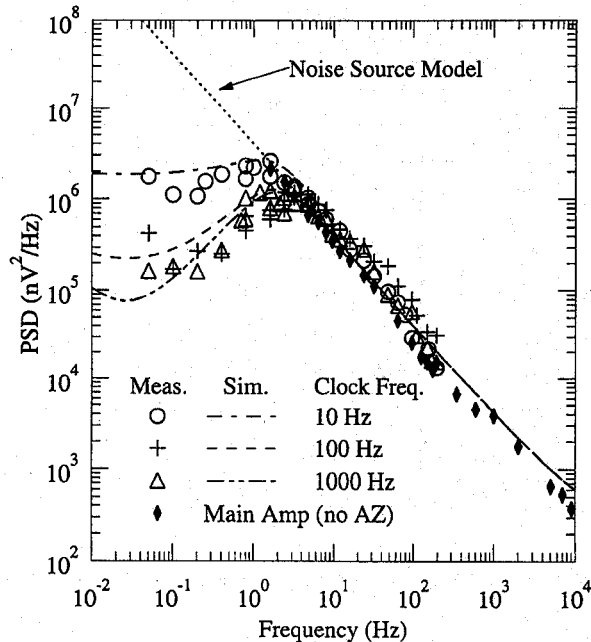


Fig. 9. Measured and simulated output noise PSD for the test amplifier with a nulling amplifier bandwidth of 2.5 Hz, corresponding to a hold capacitor of $C_{m|n} = 100$ nF. Measured data points are indicated by markers while lines are used for the calculated PSD.

TABLE I
SMALL SIGNAL MODEL PARAMETERS USED FOR SIMULATION

	Amplifier Model					Units
	1	2	3	4	5	
R_1	20	20	27	27	30.3	$M\Omega$
R_2	0.2	0.2	0.2	0.2	0.2	
R_3	20	20	14	14	30.3	
G_1	500	500	700	700	330	$\mu A/V$
G_2	5	5	43	43	3.3	
G_3	500	500	375	375	215	
G_4	500	500	300	300	330	
G_5	5	5	21	21	3.3	
C_m	100	0.9	150	150	100	nF
C_n	100	0.9	1.3	0.1	100	
C_{sh}	10	10	10	10	430	
f_s	100 [†]	100 [†]	333	1000	-	Hz
β	1	1	1	1	1	

[†] also 1000 Hz in some tests

amplifier (remembering that the main and nulling amplifiers are usually designed with identical input stages in order to minimize offset voltage).

The shape of the noise PSD at low frequencies (below the clock frequency) depends upon the effective closed loop bandwidth of the nulling amplifier, which is approximately given by $G_5/(4\pi C_m)$. When the nulling amplifier bandwidth is higher than the clock frequency, the PSD will plateau at low frequencies. Furthermore, the level of the plateau increases with increasing clock frequency, as demonstrated in Fig. 8 for $C_{m|n} = 980$ pF. For this value of hold capacitor, the

TABLE II
AMPLIFIER CHARACTERISTICS CALCULATED FROM
THE MODEL PARAMETERS GIVEN IN TABLE I

	Amplifier Model				Units
	1	2	3	4	
A_{om}	1	1	1.4	1.4	10^6
A'_{om}	10	10	87	87	10^3
A_{on}	10	10	4.2	4.2	10^3
A'_{on}	100	100	290	290	
α_m	100	100	16.3	16.3	
α_n	100	100	14.3	14.3	
GBW	0.8	0.8	0.8	0.8	MHz
$G_5/2\pi C_m$	8	884	22	22	Hz
$G_5/2\pi C_n$	8	884	2.6k	3.3k	Hz

effective gain bandwidth product of the nulling amplifier is approximately 250 Hz.

When a large hold capacitor of 100 nF is used, the nulling amplifier bandwidth decreases to about 2.5 Hz, and the PSD at low frequencies becomes almost independent of clock frequency, as illustrated in Fig. 9. Note that the clock frequency of 10 Hz approaches the bandwidth of the nulling amplifier and so the PSD begins to plateau in a similar fashion as when $C_{m|n}$ was small.

The same auto-zeroing action that reduces offset voltage also suppresses low frequency noise. At very low frequencies, $f < f_a$, the inherent noise of the nulling amplifier is suppressed by a factor of A'_{on} . Above f_a , the loop gain of the nulling amplifier begins to decrease, causing a reduction in the level of noise suppression. At the frequency of f_b the loop gain becomes unity, noise suppression ceases, and the amplifier noise is passed to the output unhindered until the pole at f_c is reached. The pole f_c is the nulling amplifier closed loop bandwidth, after which the noise PSD rolls off for higher frequencies. The noise response of the main amplifier is similar except that its bandwidth is much greater ($f_f \gg f_c$).

At very low frequencies the dominant noise contribution will come from the baseband terms. Equations (12) and (13) predict that as $f \rightarrow 0$ the output noise will be dominated by

$$\frac{S_{e_n}}{\beta A'_{on}} + \frac{S_{e_m}}{\beta A'_{on} \alpha_n / \alpha_m} \quad (27)$$

Therefore at very low frequencies the noise PSD will begin to rise at a rate proportional to the $1/f$ component of S_{e_n} and S_{e_m} . This effect can be seen in Fig. 8.

Consider in more detail the contribution to the output noise PSD of the nulling amplifier. If the nulling amplifier bandwidth is low, that is if

$$\frac{G_5}{4\pi C_n} < f_{clk} \quad (28)$$

then the low frequency PSD is nearly independent of clock frequency. This is clearly demonstrated in Fig. 9 for the case of $C_{m|n} = 100$ nF. A small dependence of the PSD on clock frequency can be seen in the change of the depth of the "valley" that occurs at approximately 0.05 Hz. The valley

is filled in by high frequency noise aliased down to baseband. The lower the clock frequency, the shallower the valley in the PSD becomes, indicating more aliased noise. As indicated by (20)–(23), as the clock frequency decreases the maximum magnitude of the transfer functions (for $x \neq 0$) for the aliased noise increases. Therefore at lower clock frequencies more noise is aliased down and it is of greater strength.

It appears that the higher the nulling amplifier bandwidth the greater the frequency range over which noise suppression can occur. This is true until a secondary limit imposed by the switched nature of the circuit is reached. This secondary limit is reached when the nulling amplifier bandwidth exceeds

$$\frac{G_5}{4\pi C_n} > \frac{4\sqrt{2}f_{clk}}{\pi} \simeq 1.8f_{clk} \quad (29)$$

after which point the effective bandwidth of the nulling amplifier becomes limited to

$$\frac{4\sqrt{2}f_{clk}}{\pi} \quad (30)$$

Attempting to increase the maximum frequency for which noise suppression occurs above the frequency specified in (30) is futile. An intuitive interpretation of this is that the sampling and subtraction process that leads to noise suppression can only occur at frequencies below the clock frequency.

For maximum low frequency noise suppression the amplifier must have a high A'_{on} (and A'_{om}) and the hold capacitors should be sized as

$$C_{m|n} = \frac{G_5}{16\sqrt{2}f_{clk}} \quad (31)$$

assuming that both the main and nulling amplifiers have identical input stages. These results suggest that to minimize the low frequency noise, an auto-zeroed amplifier should be designed with small valued hold capacitors and use a high clock frequency. This is opposite to the requirements for low input offset voltage (the primary goal of the auto-zeroed amplifier) which is reduced by using large hold capacitors and a low clock frequency [5]. Therefore the choice of capacitor size and clock frequency must reflect a compromise between noise and offset performance.

V. CONCLUSION

Periodically switched network analysis techniques have been applied to a continuous-time auto-zeroed amplifier to obtain numerical predictions of its noise behavior. From these solutions empirical expressions are developed which indicate the key design parameters that affect the noise performance. The low frequency noise is suppressed by a factor of A'_{on} , the nulling amplifier auxiliary signal path open loop gain. The maximum frequency for which noise suppression can occur is approximately the auto-zeroing clock frequency; however, if the nulling amplifier bandwidth is below the clock frequency then the noise suppression will cease at the bandwidth frequency. The nulling amplifier bandwidth also affects the shape of the low frequency output noise

$$H_x(f) = e^{j\pi x\chi} \text{sinc}(x\chi) - \frac{\chi e^{-j\pi\chi(f/f_{\text{clk}} - 2x)} \sin(\pi\chi f/f_{\text{clk}}) (1 - e^{-\frac{1-x}{f_{\text{clk}}}\left(\frac{1}{RC} + j2\pi(f-xf_{\text{clk}})\right)})}{(1 + j2\pi RC(f - xf_{\text{clk}})) \left(1 - e^{-\frac{1-x}{f_{\text{clk}}}\left(\frac{1}{RC} + j\frac{2\pi(f-xf_{\text{clk}})}{1-x}\right)}\right)} \quad (34)$$

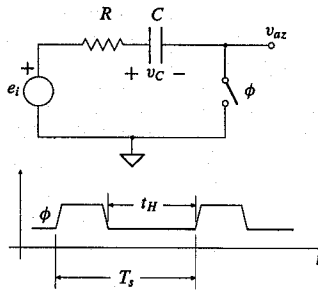


Fig. 10. A simplified model of a discrete-time auto-zeroed amplifier.

PSD. If the bandwidth is above the clock frequency, the low frequency PSD will show a flat plateau, the level of which will rise with decreasing clock frequency. If the bandwidth is below the clock frequency, the low frequency PSD will have a humped plateau that is largely independent of clock frequency. Independent of the nulling amplifier bandwidth, the PSD at very low frequencies will begin to rise again at a rate proportional to $1/f$. For frequencies greater than the clock frequency, the output PSD will be dominated by the contribution of the main amplifier inherent noise source.

APPENDIX

DISCRETE-TIME AUTO-ZEROED AMPLIFIER

A simplified model of a bandwidth limited discrete-time auto-zeroed amplifier is shown in Fig. 10. This circuit is simple enough that the switched network analysis methods of Strom and Signell can be applied to determine an exact analytic solution for the output frequency response.

The total output noise PSD due to the noise source e_i with a spectral density S_i is given by

$$S_{AZ}(f) = \sum_{x=-\infty}^{\infty} |H_x(f)|^2 S_i(f - xf_{\text{clk}}) \quad (32)$$

where the transfer functions are labeled H_x in order to clearly differentiate them from the transfer functions T_x used for the continuous-time auto-zeroed amplifier.

It can be shown that for $x = 0$ the transfer function is given by

$$H_0(f) = \chi \left[1 - \frac{e^{-j\pi\chi f/f_{\text{clk}}} \sin(\pi\chi f/f_{\text{clk}}) (1 - e^{-\frac{1-x}{f_{\text{clk}}}\left(\frac{1}{RC} + j2\pi f\right)})}{(1 + j2\pi f RC) \left(1 - e^{-\frac{1-x}{f_{\text{clk}}}\left(\frac{1}{RC} + j\frac{2\pi f}{1-x}\right)}\right)} \right] \quad (33)$$

and for $x \neq 0$ (see (34) at the top of the page) where f_{clk} is the sampling frequency, and $\chi = t_H/T_s$ is the ratio of the hold time t_H to the sampling period T_s (see Fig. 10).

If $R \rightarrow 0$, then (33)–(34) reduce to

$$|H_0(f)|^2 = \chi^2 [1 + \text{sinc}^2(\chi f/f_{\text{clk}}) - 2 \cos(\pi\chi f/f_{\text{clk}}) \text{sinc}(\chi f/f_{\text{clk}})] \quad (35)$$

and

$$|H_x(f)|^2 = \chi^2 [\text{sinc}^2(\chi f/f_{\text{clk}}) + \text{sinc}^2(x\chi) + 2 \text{sinc}(\chi f/f_{\text{clk}}) \times \text{sinc}(x\chi) \cos(\pi\chi(f/f_{\text{clk}} - x))] \quad (36)$$

which, for $\chi = 1$, are similar to the expressions obtained by Enz in [10] for a simplified discrete-time auto-zeroed amplifier. The transfer functions shown in (35) and (36) are more general than those given by Enz in [10] since an infinitely short sampling time (i.e., $\chi = 1$) is not assumed.

ACKNOWLEDGMENT

IC design and test facilities along with fabrication services were provided by the Canadian Microelectronics Corporation.

REFERENCES

- [1] M. C. Coln, "Chopper stabilization of MOS operational amplifiers using feed-forward techniques," *IEEE J. Solid-State Circuits*, vol. SC-16, pp. 745–748, Dec. 1981.
- [2] E. A. Vittoz, "Dynamic analog techniques," in *Design of MOS VLSI Circuits for Telecommunication*, Y. Tividis and P. Antognetti, Eds. Englewood Cliffs, NJ: Prentice-Hall, 1985, pp. 145–170, ch. 5.
- [3] P. M. V. Peteghem, I. Verbuuwhe, and W. M. Sansen, "Micropower high-performance SC building block for integrated low-level signal processing," *IEEE J. Solid-State Circuits*, vol. SC-20, pp. 837–844, Aug. 1985.
- [4] I. G. Finvers, J. W. Haslett, and F. N. Trofimenkoff, "A high temperature precision amplifier," *IEEE J. Solid-State Circuits*, vol. SC-30, pp. 120–128, Feb. 1995.
- [5] I. G. Finvers, "A CMOS high temperature auto-zeroed amplifier," Ph.D. dissertation, Univ. Calgary, 1995.
- [6] M. H. White, D. R. Lampe, F. C. Blaha, and I. A. Mack, "Characterization of surface channel CCD image arrays at low light levels," *IEEE J. Solid-State Circuits*, vol. SC-9, pp. 1–13, Feb. 1974.
- [7] R. J. Kansy, "Response of a correlated double sampling circuit to $1/f$ noise," *IEEE J. Solid-State Circuits*, vol. SC-15, pp. 373–375, June 1980.
- [8] H. Wey and W. Guggenbuhl, "Noise transfer characteristics of a correlated double sampling circuit," *IEEE Trans. Circuits Syst.*, vol. CAS-33, pp. 1028–1030, Oct. 1986.
- [9] A. Rizzi, "N-delta and differential average signal processors: Detailing of their signal and noise response," *IEEE J. Solid-State Circuits*, vol. SC-28, pp. 49–58, Jan. 1993.
- [10] C. Enz, "Analysis of low-frequency noise reduction by autozero technique," *Electron. Lett.*, vol. 20, pp. 959–960, Nov. 1984.
- [11] M. L. Liou, Y. Long Kuo, and C. F. Lee, "A tutorial on computer-aided analysis of switched-capacitor circuits," *Proc. IEEE*, vol. 71, pp. 987–1005, Aug. 1983.
- [12] M. L. Liou, "Exact analysis of linear circuits containing periodically operated switches with applications," *IEEE Trans. Circuit Theory*, vol. CT-19, pp. 146–154, Mar. 1972.
- [13] T. Strom and S. Signell, "Analysis of periodically switched linear circuits," *IEEE Trans. Circuits Syst.*, vol. CAS-24, pp. 531–541, Oct. 1977.

- [14] M. Aaron, "Application, characterization, and design of switched filters," in *Modern Filter Theory and Design*, G. C. Temes and S. K. Mitra, Eds. New York: Wiley, 1973, pp. 415-463.
- [15] R. Gregorian and G. C. Temes, *Analog MOS Integrated Circuits for Signal Processing*. New York: Wiley, 1986.
- [16] K. R. Laker and W. M. Sansen, *Design of Analog Integrated Circuits and Systems*. New York: McGraw-Hill, 1994.
- [17] H. A. Haus and R. B. Adler, "Invariants of linear noisy networks," *IRE Conv. Rec.*, vol. 4, pp. 53-67, 1956.
- [18] Y. P. Tsividis, *Operation and Modeling of the MOS Transistor*. New York: McGraw-Hill, 1987.
- [19] S. Daubert, "Noise in switched-current circuits," in *Switched-Currents an Analogue Technique for Digital Technology*, C. Toumazou, J. Hughes, and N. Battersby, Eds. London, U.K.: Peter Peregrinus, 1993, pp. 136-155, ch. 5.
- [20] G. Wegmann, "Dynamic current mirrors," in *Switched-Currents an Analogue Technique for Digital Technology*, C. Toumazou, J. Hughes, and N. Battersby, Eds. London, U.K.: Peter Peregrinus, 1993, pp. 404-455, ch. 16.
- [21] J. A. Kaelher, "Periodic-switched filter networks—A means of amplifying and varying transfer functions," *IEEE J. Solid-State Circuits*, vol. SC-4, pp. 225-230, Aug. 1969.



Ivars G. Finvers received the B.Sc. and M.Sc. degrees in electrical engineering from the University of Alberta in 1985 and 1988, respectively. In 1994, he received the Ph.D. degree from the University of Calgary, where he developed high performance CMOS operational amplifiers for high temperature instrumentation applications.

From 1985 to 1986 he was a Member of Scientific Staff at Bell Northern Research engaged in the development of test equipment for fiber optic system installation and monitoring. In 1988 he joined

NovAtel Communications Ltd. as an IC design/test engineer responsible for the design, simulation, testing, and support of custom integrated circuits for cellular telephony applications. Since the beginning of 1995 he has been with Mitel Semiconductor, Ottawa, Ontario, Canada, where he is involved in all aspects of the design, testing, and production of standard product telecommunication IC's.

Dr. Finvers is a member of the Association of Professional Engineers, Geologists and Geophysicists of Alberta.

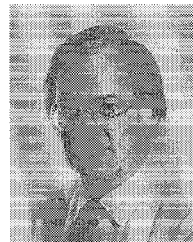


James W. Haslett (S'64-M'66-SM'79) received the B.Sc. degree in electrical engineering from the University of Saskatchewan in 1966, and the M.Sc. and Ph.D. degrees from the University of Calgary in 1968 and 1970, respectively.

He subsequently joined the Department of Electrical Engineering at the University of Calgary, where he is currently Professor and head of the Department. His current research interests include optical imaging systems for spacecraft applications, instrumentation systems related to drill-stem testing

of oil and gas wells, high temperature semiconductor device behavior, and the design of analog and digital VLSI circuits.

Dr. Haslett is a member of the Association of Professional Engineers, Geologists and Geophysicists of Alberta, the Canadian Astronomical Society, the Canadian Society of Exploration Geophysicists, and the American Society for Engineering Education.



F. N. Trofimenkoff (M'63-SM'69) was born in Veregin, Saskatchewan, Canada on August 10, 1934. He received the B.E. degree in engineering physics and the M.Sc. degree in physics, both from the University of Saskatchewan, Saskatoon, Canada in 1957 and 1959, respectively. He was awarded an Athlone Fellowship in 1959 and received the Ph.D. degree in electrical engineering (semiconductor device physics) from the University of London at the Imperial College of Science and Technology, London, England in 1962.

From 1957 to 1959, he worked on instrumentation for accurate humidity measurement in the Division of Building Research of the National Research Council of Canada, and from 1962 to 1966 he was an Assistant Professor of Electrical Engineering at the University of Saskatchewan. In 1966, he moved to the Electrical Engineering Department of the University of Calgary, Alberta, Canada. His current interests are in the circuits and devices area and in instrumentation related to the petroleum industry.

Dr. Trofimenkoff is a member of the Association of Professional Engineers, Geologists and Geophysicists of Alberta, the Engineering Institute of Canada, the Canadian Association of Physicists, the Canadian Society of Exploration Geophysicists and the American Society for Engineering Education.